JOURNAL OF APPLIED PHYSICS VOLUME 93, NUMBER 8 15 APRIL 2003

Determination of texture by infrared spectroscopy in titanium oxide–anatase thin films

Carlos Pecharromán[a)]
Instituto de Ciencia de Materiales de Madrid, CSIC, Cantoblanco, 28049 Madrid, Spain

Francisco Gracía, Juan P. Holgado, Manuel Ocaña, and Agustín R. González-Elipe
Instituto de Ciencia de Materiales de Sevilla (CSIC-University Sevilla), Avda Américo Vespucio s/n, 41092 Sevilla, Spain

J. Bassas
Serveis Cientificotècnics de la U.B., Solé i Sabarís, 1-3, 08028 Barcelona, Spain

J. Santiso and A. Figueras
Institut de Ciència de Materials de Barcelona-CSIC, 08193 Bellaterra, Spain

(Received 29 May 2002; accepted 21 January 2003)

A theoretical model to determine the effective dielectric tensor of heterogeneous materials composed by anisotropic microcrystallites has been introduced to explain the infrared spectral features of textured thin films of uniaxial materials as the function of a textural parameter. This theoretical treatment is able to satisfactorily reproduce the experimental absorbance spectra of TiO_2–anatase thin films chosen as a model system. Comparison of texture data obtained from infrared spectroscopy and x-ray diffraction are in good agreement which support the validity of the proposed model. © *2003 American Institute of Physics.* [DOI: 10.1063/1.1560858]

I. INTRODUCTION

Infrared absorption/reflection infrared (IR) spectroscopy on thin films is commonly used as an analytic technique to identify the nature of the deposited materials. When done at normal incidence, transverse optical phonons of isotropic compounds can be detected as absorption maxima, while at grazing angles and perpendicular polarization these modes vanish substituted by longitudinal optical phonons. This effect, firstly reported by Berreman,[1] has been widely used to experimentally determine the longitudinal frequencies of several cubic substances.[2,3] However, in the case of anisotropic samples, this effect is only verified under very restrictive conditions, which depend on the orientation of the optical axes of the layer. In fact, in anisotropic layers pure longitudinal or transverse phonons[4] only propagates in very specific directions, related with the optical axes of the crystal.

Most thin film growth techniques produce polycrystalline films. The physical properties of these layers can be considered isotropic (at a length scale larger than the crystallite size) even or anisotropic materials if the crystallites are randomly distributed and oriented. The optical properties of highly diluted composites of these materials can be calculated by an effective dielectric constant approximation[5] and the original Berreman's formulation[1] can still be used. However, this approximation fails in anisotropic substances when the preparation procedure introduces a preferential texture, i.e., when the film depicts a preferential orientation of some of their crystal planes. In these cases, thin films behave as anisotropic media.

Preferential texturing of thin films is easily identified by x-ray diffraction (XRD) in a Bragg–Brentano configuration because the diffraction peaks of the planes preferentially oriented according to the thin film surface present an enhanced intensity.

There is some previous publications which tried to link the effective[6] and average[7,8] dielectric constant with textural parameters, but there is not a systematic treatment of this subject. In a previous publication, we used a qualitative approach by Fourier transform IR spectroscopy (FT-IR) to deduce preferential orientation phenomena in Fe_2O_3 pressed pellets[9] and thin films.[10] In the present article we introduce a theoretical treatment of FT-IR spectra of thin films that enables us to gain information about the preferential orientation of crystal planes. For a sake of simplicity we have restrict the range of application of this model to uniaxial compounds, i.e., those that crystallize into the tetragonal, rhombohedral, and hexagonal systems, but the extension to biaxial ones is straightforward. To verify the possibilities of the model, characterization experiments by FT-IR, with polarized and unpolarized light, and XRD of TiO_2 anatase thin films have been carried out. The good concordance of the results by the two techniques, indicating the preferential orientation of a given type of crystal planes, has confirmed the predictions of the model and open the possibility of systematically using FT-IR for proving preferential orientation phenomena in thin films.

II. EXPERIMENT

Very compact and dense TiO_2 thin films have been prepared by ion beam induced chemical vapor deposition. A thorough description of this procedure can be found in a previous publication.[11] Briefly, it consists of inducing the decomposition of a volatile precursor of the metal (in this

[a)]Author to whom correspondence should be addressed; electronic mail: cpg@icmm.csic.es

case Ti) with a beam of accelerated O_2^+ ions. Here, Ti isopropoxide has been used as volatile precursor of Ti and the beam energy and current at the substrate position were 400 eV and 100 μA cm^{-2}, respectively. They were grown at room temperature on a flat Si (100) substrate. The film thickness was 450 nm. After preparation, the films were amorphous but they crystallized into the anatase structure of TiO_2 after annealing in air at $T \geqslant 300\,°C$. Samples annealed at 300 and 600 °C were studied by XRD and FT-IR (hereafter these samples will be called TiO_2-300 and TiO_2-600).

X-ray powder diffraction patterns were obtained in a Bragg–Brentano $\theta/2\theta$ diffractometer, Siemens D500; a divergence slit of 1° was used, resulting on an incident beam of 3.8 mm at the sample position. The Cu $K\alpha$ radiation was used as excitation source at a working power of 40 kV×30 mA.

FT-IR spectra with unpolarized light were recorded from 200 to 1000 cm^{-1} in the transmission mode in a Nicolet 510 Fourier transform spectrometer. FT-IR spectra with polarized light were recorded 400–1000 cm^{-1} in a Nicolet 20 SXC by using a wire KBr polarizer. The angle between the beam and the normal to the thin film surface was changed for different measurements.

III. THEORETICAL PROCEDURE

A. Effective medium approximation for dielectric composites

In contrast to isotropic polycrystalline materials, the optical properties of dense anisotropic solids can be substantially different from those of single crystals, as a consequence of the decisive role of the orientation of the crystallites in these materials. Thus, a sort of average of the optical properties of the single crystallites along different directions of the dielectric tensor should be expected in macroscopic samples. In order to properly calculate the properties of these materials, an effective medium theory has been introduced, based on an effective medium formalism developed by the authors in some previous publications.[9,12] This approach, which can be considered as a generalization of several others models previously presented,[5,13,14] was formulated for isotropic and anisotropic particles randomly distributed into a heterogeneous material, in such a way that the whole composite presents an isotropic macroscopic behavior. In this context, it was assumed for the isotropic case that the average electric field in the vicinity of the particles was constant, homogeneous and identical to the average electric field $\langle E\rangle_{\mathbf{E}_0}$, (effective medium theory). In addition, it is supposed that particle shape is ellipsoidal, so that the electric field inside this particles is also constant and can be easily calculated. However, when crystallites present textured distributions, the composite may be anisotropic and in this case the electric field inside of a ellipsoidal article is no longer isotropic nor homogeneous even if the external field is assumed to be homogeneous. However, a detailed calculation shows (Appendix A) that although the heterogeneous medium can display an anisotropic behavior, each component of the macroscopic effective dielectric tensor along its optical axes can be reasonably approximated by an effective medium approximation. Thus, according to Refs. 12 and 9, and the conclusions obtained in Appendix A, the general equation which determines the effective dielectric constant of a heterogeneous composite formed by two anisotropic phases (labeled by subindex "p" and "m") along the direction l, is given by:

$$\langle\epsilon\rangle_l = \frac{(1-f)\sum_{k=1}^{3}\frac{c_{mkl}\epsilon_{mk}}{(1-L_{mk})\langle\epsilon\rangle_l + L_{mk}\epsilon_{mk}} + f\sum_{k=1}^{3}\frac{c_{pkl}\epsilon_{pk}}{(1-L_{pk})\langle\epsilon\rangle_l + L_{pk}\epsilon_{pk}}}{(1-f)\sum_{k=1}^{3}\frac{c_{mkl}}{(1-L_{mk})\langle\epsilon\rangle_l + L_{mk}\epsilon_{mk}} + f\sum_{k=1}^{3}\frac{c_{pkl}}{(1-L_{pk})\langle\epsilon\rangle_l + L_{pk}\epsilon_{pk}}}, \tag{1}$$

where subindex k refers to the axes (x, y and z), which for spheroidal shapes, are restricted to x and z; f is the filling factor, L_{mk} and L_{pk} the depolarization factors of the matrix and particle spheroids along the k axis, and c_{mkl} and c_{pkl} the average of the projection of a unit vector parallel to the optic axis onto the applied electric field.

B. Application of the effective medium approximation to dense materials

In the case of a dense aggregate, i.e., $f=1$, the m phase is absent so that it can be dropped from Eq. (1). Then the effective dielectric constant along the l axis notably simplify into:

$$\sum_{k=1}^{3}\frac{c_{pkl}(\epsilon_{pk}-\langle\epsilon\rangle_l)}{(1-L_{pk})\langle\epsilon\rangle_l + L_{pk}\epsilon_{pk}} = 0. \tag{2}$$

It should be noted that these expressions of the effective dielectric tensor components depend on geometrical factors of the crystalline grains, i.e., the grain shape through L_{pk} and on the average orientation given by c_{pkl}. In this sense, any texture effect on the IR spectra should be well described by these coefficients. In order to greatly simplify the notation, we have assumed that crystallites are optically uniaxial so that each crystallite has its own optical axis (denoted by "o" and "e" for ordinary and extraordinary rays), which defines an angle θ with the z axis of the layer. If cylindrical symmetry is assumed for the thin layer, it must become optically uniaxial, being $\langle\epsilon\rangle_z$ the dielectric constant along the z axis

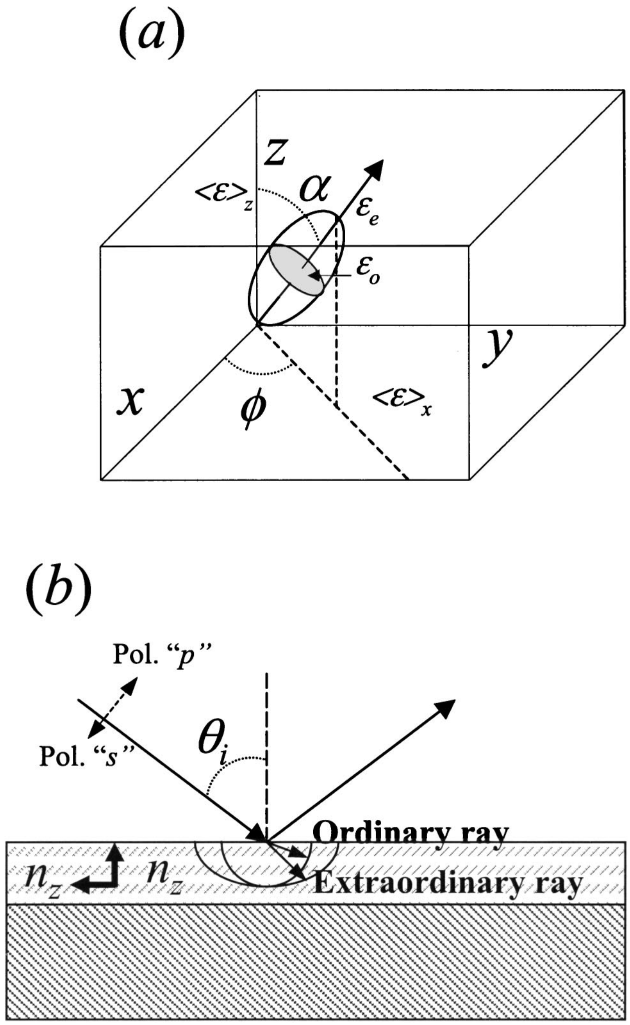

FIG. 1. (a) Geometry of an ellipsoidal particle in the layer frame; (b) geometry of a plane thick layer.

and $\langle \epsilon \rangle_x$ that corresponding to the $x-y$ plane. The relationships between optical axes of the composite, x and z, with those of the crystallite can be deduced from Fig. 1(a). Using the definition of c_{pkl} enclosed in Eq. (1) as it appears in Appendix A, we get the analytic expression of these geometric coefficients

$$c_{\text{pex}} = 1/4\pi \int \sin^2(\theta)\gamma_{\text{pe}}(\theta) d\Omega, \tag{3}$$

$$c_{\text{pez}} = 1/4\pi \int \cos^2(\theta)\gamma_{\text{pe}}(\theta) d\Omega, \tag{4}$$

$$c_{\text{pox}} = 1/4\pi \int \sin^2(\theta)\gamma_{\text{po}}(\theta) d\Omega, \tag{5}$$

$$c_{\text{poz}} = 1/4\pi \int \cos^2(\theta)\gamma_{\text{po}}(\theta) d\Omega, \tag{6}$$

where $d\Omega$ is the solid angle differential, and γ_{pe} and γ_{po} are the probability density function corresponding to the angular orientation of the extraordinary and ordinary optical axis. It should be noted that the terms $\sin^2(\theta)$ and $\cos^2(\theta)$ in Eqs. (3)–(6) are obtained as a result of the projection of each component of the dielectric tensor to $\gamma_{kl,\mathbf{E}_0}(\theta)$, i.e., the density function corresponding to the probability of finding that the l axis of the ellipsoid makes an angle θ with $\mathbf{E}_0$. Due to the fact that axial symmetry has been assumed along the perpendicular to the sample surface, then, γ_{pe} and γ_{po} only depend on the angle θ. Moreover, in uniaxial substances the ordinary axes are degenerated into a plane, then

$$\frac{2\int \gamma_{\text{po}} d\Omega + \int \gamma_{\text{pe}} d\Omega}{4\pi} = 1. \tag{7}$$

Thus we get the following relationships between the four different coefficients:

$$\begin{cases} 2c_{\text{pox}} + c_{\text{pex}} = 1 \\ 2c_{\text{poz}} + c_{\text{pez}} = 1 \\ 2c_{\text{pox}} + c_{\text{poz}} = 1 \\ 2c_{\text{pex}} + c_{\text{pez}} = 1. \end{cases} \tag{8}$$

If we consider that c_{pez} can take any value from 0 to 1, then Eqs. (8) impose the limiting conditions for the rest of the c coefficients

$$\begin{cases} c_{\text{pez}} = 0...1 \\ c_{\text{pex}} = \dfrac{1-c_{\text{pez}}}{2} = \dfrac{1}{2}\ldots 0 \\ c_{\text{poz}} = \dfrac{1-c_{\text{pez}}}{2} = \dfrac{1}{2}\ldots 0 \\ c_{\text{pox}} = \dfrac{1+c_{\text{pez}}}{4} = \dfrac{1}{4}\ldots\dfrac{1}{2}. \end{cases} \tag{9}$$

At this point it is possible to simplify Eq. (2) to obtain two expressions for determining the effective dielectric constant along the x and z axes

$$\frac{(1+c_{\text{pez}})}{2} \frac{(\langle \epsilon \rangle_x - \epsilon_{\text{po}})}{(1-L_{\text{po}})\langle \epsilon \rangle_x + L_{\text{po}}\epsilon_{\text{po}}} + \frac{(1-c_{\text{pez}})}{2} \frac{(\langle \epsilon \rangle_x - \epsilon_{\text{pe}})}{2L_{\text{po}}\langle \epsilon \rangle_x + (1-2L_{\text{po}})\epsilon_{\text{pe}}} = 0, \tag{10}$$

$$(1-c_{\text{pez}}) \frac{(\langle \epsilon \rangle_z - \epsilon_{\text{po}})}{(1-L_{\text{po}})\langle \epsilon \rangle_z + L_{\text{po}}\epsilon_{\text{po}}} + c_{\text{pez}} \frac{(\langle \epsilon \rangle_z - \epsilon_{\text{pe}})}{2L_{\text{po}}\langle \epsilon \rangle_z + (1-2L_{\text{po}})\epsilon_{\text{pe}}} = 0. \tag{11}$$

These expressions look very similar to that obtained in the well known Bruggemann effective medium theory.[15,16] That approximation was formulated for heterogeneous media composed by two isotropic phases, being f the volume concentration of one of them. In our model the composite only has one single anisotropic phase but two different components of the dielectric tensor. In this case the role of the phases is replaced with the dielectric tensor components of crystallites. Moreover, the role of the volume concentration, f, is assumed in a dense anisotropic composite by two expressions related to the orientation coefficient c_{pez}. It should be noted that Eqs. (10) and (11) are two second degree equations in $\langle \epsilon \rangle_x$ and $\langle \epsilon \rangle_z$.

$$a_x \langle \epsilon \rangle_x^2 + \langle \epsilon \rangle_x (\epsilon_o b_{ox} + \epsilon_e b_{ex}) - \epsilon_e \epsilon_o c_x = 0, \tag{12}$$

$$a_z \langle \epsilon \rangle_z^2 + \langle \epsilon \rangle_z (\epsilon_o b_{oz} + \epsilon_e b_{ez}) - \epsilon_e \epsilon_o c_z = 0. \tag{13}$$

TABLE I. Effective dielectric constant, anisotropic character, and weight of each kind of phonon (transverse, longitudinal, ordinary, and extraordinary) in the absorption spectrum as a function of the crystallite orientation angle.

α	c_{pez}	ϵ_x	ϵ_z	Anisotropy	$W(\omega_{TO})$ $\theta_i=0°$	$W(\omega_{LO})$ $\theta_i=90°$	$W(\omega_{TE})$ $\theta_i=0°$	$W(\omega_{LE})$ $\theta_i=90°$
90°	0	$\frac{\epsilon_o+\epsilon_e}{2}$	ϵ_o	Yes	1/2	1/2	1	0
45° or random	1/3	$\frac{2\epsilon_o+\epsilon_e}{3}$	$\frac{2\epsilon_o+\epsilon_e}{3}$	No	2/3	1/3	2/3	1/3
0°	1	ϵ_o	ϵ_e	Yes	1	0	0	1

The coefficients of these equations are given by

$$\begin{cases} a_x=1+L_p+c_{\mathrm{pez}}(-1+3L_p) \\ b_{ox}=-L_p-3c_{\mathrm{pez}}L_p \\ b_{ex}=-L_p+2c_{\mathrm{pez}}-3c_{\mathrm{pez}}L_p \\ c_x=1-L_p+c_{\mathrm{pez}}(1-3L_p), \end{cases} \tag{14}$$

$$\begin{cases} a_z=2L_p+c_{\mathrm{pez}}(1-3L_p) \\ b_{oz}=-2L_p+3c_{\mathrm{pez}}L_p \\ b_{ez}=1-2L_p-2c_{\mathrm{pez}}+3c_{\mathrm{pez}}L_p \\ c_z=1-2L_p-c_{\mathrm{pez}}(1-3L_p). \end{cases} \tag{15}$$

To illustrate the relationship between these coefficients with textural parameters given by γ_{pe}, [Eqs. (3)–(6)] let us consider two extreme cases: (i) a layer made by crystallites randomly oriented and (ii) a layer formed by crystallites totally oriented towards a specific orientation, which describes an angle α with the layer normal.

In the first case $\gamma_{\mathrm{pe}}(\theta)$ is a constant independent of θ, so that $c_{\mathrm{pez}}=c_{\mathrm{pex}}=1/3$ and according to Eqs. (10) and (11) the heterogeneous medium presents an isotropic behavior ($\langle\epsilon\rangle_x=\langle\epsilon\rangle_z$). This results coincides with the isotropic previous models.[13,14] In the second case, the function $\gamma_{\mathrm{pe}}(\theta)$ can be written as a Dirac's delta

$$\gamma_{\mathrm{pe}}(\theta)=g\cdot\delta(\theta-\alpha), \tag{16}$$

where g is the normalization constant. By using Eq. (4) we get:

$$c_{\mathrm{pez}}=g\int_0^{\pi/2}\cos^2(\theta)\sin(\theta)\,\delta(\theta-\alpha)\,d\theta$$
$$=g\cos^2(\alpha)\sin(\alpha). \tag{17}$$

The coefficient c_{pex} can be obtained operating in the same way with Eq. (3). Then, by using Eq. (8), it is possible to determine g to get the final expression of c_{pez} as a function of α.

$$c_{\mathrm{pez}}(\alpha)=\frac{\cos^2(\alpha)}{1+\sin^2(\alpha)}. \tag{18}$$

Equations (10) and (11) in combination with Eq. (18) allow us to relate the optical anisotropy of the polycrystalline material with the angle of preferential orientation. Assuming a quasispherical particular shape ($L_p=1/3$), we can state that different anisotropy schemes (Table I) could appear in a polycrystalline anisotropic material as a function of the orientation coefficient c_{pez}.

If all the crystallographic axes of the crystallites are perpendicularly oriented to the normal of the surface sample, i.e., α=90° then, by using Eq. (18), it results that $c_{\mathrm{pez}}=0$. The substitution of this value in Eqs. (10) and (11) determines that $\langle\epsilon_x\rangle$, the dielectric tensor coefficient corresponding to the plane parallel to the surface sample, is equal to the arithmetic mean value of ordinary and extraordinary components of crystallites (ϵ_o and ϵ_e), while the $\langle\epsilon_z\rangle$ component is identical to the ordinary one of the microcrystals (ϵ_o). Thus, the absorbance IR spectrum detected for the sample under normal incidence will be a combination of transverse modes of the ordinary and extraordinary rays. However by tilting the sample, longitudinal modes of the ordinary ray begin to appear, while longitudinal modes of the extraordinary component remain absent.

On the contrary, if all the crystallites axes are perpendicular to the sample surface we get α=0°, and $c_{\mathrm{pez}}=1$. This geometric configuration is identical, from an optical point of view, to that of a single (anisotropic) crystal with its optical axis parallel to the normal to the crystal surface. Under these circumstances, we must observe the transverse ordinary modes by IR absorption spectroscopy at normal incidence, while only the longitudinal extraordinary modes must be detected at grazing angles.

Finally, if crystallites are randomly oriented, according to Eq. (4), it results that $c_{\mathrm{pez}}=1/3$, a value which coincides with that of crystallite axes oriented 45° with respect to the normal to the plane. Under these conditions, Eqs. (10) and (11) determine that the whole sample behaves as an isotropic material, being identical to all the components of the dielectric tensor. It should be noted that this angle is different from the so called "magic angle" [$\cos^2(\theta_M)=1/3$ or $\theta_M=54°44'$] which corresponds to an angular average of the considered magnitude[7,8] (permittivity, refractive index, reflectivity, etc). The discrepancy in our case is due to the fact that the calculation of effective dielectric constant takes into account the projection of the internal field of the particles (which in our case satisfies the conditions of magic angle) over the xy plane and the z axis, instead of the average permittivity tensor.

These results are the limit cases that can appear in a dense anisotropic polycrystalline material. Thus, they can be used as a quick test to detect texture in polycrystalline thin layers measured by IR absorption spectra at normal and grazing angles.

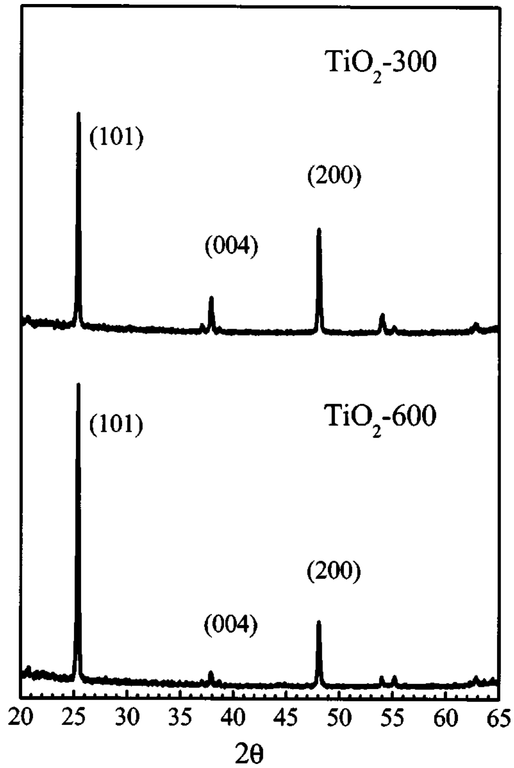

FIG. 2. XRD of anatase thin films prepared at 300 and 600 °C.

However, a quantitative evaluation of the optical properties of anisotropic thin layers is somehow more complicated[17] and requires the use of the 4×4 transfer matrix formulation.[18,19] This method has been recently employed in ellipsometry in order to determine the optical constants of single crystal anisotropic layers.[20–22] We have used the explicit formulation given by Schubert[23] as it appears in Appendix B.

Once the full set of equations is implemented we get a calculation procedure which is able to estimate the theoretical spectra of dense heterogeneous anisotropic thin layers, where anisotropy is a consequence of preferential orientation of its crystallites. In order to obtain its theoretical spectrum the following data are necessary: thickness of the layer, incidence angle and polarization degree of incident beam, refractive index of microparticles, usually measured on single crystals, approximate shape of crystallites (L_p), and orientation degree (c_{pez}).

It is clear that a dense material composed by anisotropic grains can present a rich variety of different spectra especially if ϵ_o and ϵ_e have large differences in a wide spectral range.

IV. RESULTS

A. Textural analysis of TiO_2 thin films by XRD

The XRD patterns corresponding to the two samples studied here (i.e., TiO_2-300 and TiO_2-600) are shown in Fig. 2. The two diagrams show a diffraction pattern typical of that of anatase. For a comparative analysis of the two diagrams,

TABLE II. Intensities, normalization factors, and corrected intensities of the diffraction peaks of anatase thin films.

		TiO_2-300 ($\tau=0.45$ μm), $2\theta_L=42.0°$)				TiO_2-600 ($\tau=0.32$ μm $2\theta_L=49.4°$)			
hkl	2θ	C_{hkl}	I^{obs}	I^c	R^c	C_{hkl}	I^{obs}	I^c	R^c
101	25.308	1.000	53.0	1214	1.000	1.000	73.0	2352	1.000
004	37.791	1.000	11.0	252	0.208	1.000	4.0	129	0.055
200	48.047	1.137	34.0	886	0.730	1.000	21.0	677	0.288
105	53.885	1.265	7.5	217	0.179	1.084	2.5	87	0.037
211	55.073	1.291	1.8	53	0.044	1.106	3.3	118	0.050
204	62.692	1.452	3.0	99	0.082	1.245	2.5	132	0.056

the observed integrated intensities (I^{obs}) of the main reflections are corrected by taking into account both layer thickness and sample size:

$$\frac{I^c}{I^{\text{obs}}}=\frac{C_{hkl}}{2\mu\tau}, \tag{19}$$

where C_{hkl} is a normalization factor calculated as $C_{hkl}=\sin\theta/\sin\theta_L$ (if $\theta>\theta_L$); and $C_{hkl}=1$ (if $\theta<\theta_L$); the incident angle cutoff, θ_L, depends on the sample size and the incident beam cross section ($\theta_L=21.0°$ and 24.7° for the TiO_2-300 and TiO_2-600 samples respectively); τ, the layer thickness and the absorption coefficient for TiO_2–anatase, is $\mu=0.0485\ \mu\text{m}^{-1}$.

Observed and corrected intensities are indicated in Table II, as well as the relative corrected intensities $(R^c=I^c/I^c_{101})$ referred to the 101 reflection.

The degree of orientation for a given diffracting plane can be calculated considering the deviation from the relative corrected intensities with respect to the same planes in a random distributed anatase. The used coefficient Q_{hkl} is

$$Q_{hkl}=\frac{R^c_{hkl}}{\beta_{hkl}}-1, \tag{20}$$

where β means the relative integrated intensity of the hkl reflection with respect the 101 one (100%) when the material is randomly oriented.

The relative density of planes of a given orientation, N_{hkl}, can be also estimated from relative corrected intensities, using the normalized expression

$$N_{hkl}=\frac{R^c_{hkl}/\beta_{hkl}}{\Sigma^{i=1}_{N_{mx}}R^i_c/\beta_i}, \tag{21}$$

where the summation extends over all the considered reflections along the diffraction pattern. For the present work, we have considered $N_{mx}=6$ different reflections, as it appears in Table II. Consequently, $N_{hkl}=1/6$ would correspond to a random orientation and $N_{hkl}>1/6$ indicates that (hkl) planes are preferentially oriented parallel to the sample surface, the higher the value the stronger the orientation.

The Q_{hkl} and N_{hkl} values obtained for both samples studied are summarized in the Table III. As observed, the most significant difference between the two samples regarding the relative orientation of their crystallographic planes corresponds to the (101) plane. In fact, this plane has N_{hkl}

TABLE III. Texture parameters of the TiO_2 samples.

		TiO_2-300			TiO_2-600		
hkl	β_{hkl}	R^c_{hkl}	Q_{khl}	N_{hkl}	R^c_{hkl}	Q_{khl}	N_{hkl}
101	1.000	1.000	0.00	0.16	1.000	0.00	0.32
004	0.206	0.208	0.01	0.16	0.055	−0.73	0.09
200	0.290	0.730	1.52	0.40	0.288	−0.01	0.32
105	0.188	0.179	−0.05	0.15	0.037	−0.80	0.06
211	0.187	0.044	−0.76	0.04	0.050	−0.73	0.09
204	0.148	0.082	−0.45	0.09	0.056	−0.62	0.12

values of 0.16 and 0.32 in the TiO_2-300 and TiO_2-600 samples, respectively. These values indicate that while this family of planes is randomly oriented in the first sample, it presents a clear preferential orientation parallel to the thin film surface in the second sample. A smaller change (i.e., from 0.40 to 0.32) in the N_{hkl} value is also found for the (200) planes when comparing the two samples, although in the two cases the parameter was almost double that of 0.16, the typical value of a randomly oriented sample. This means that in the two samples the (200) family of planes is preferentially oriented parallel to the thin film surface and that there are no significant differences between them in the relative orientation degree. For the (004) planes the situation is the opposite since these planes lose orientation degree when comparing the TiO_2-300 with the TiO_2-600 samples (i.e., N_{hkl} values of 0.16 and 0.09). The other reflections whose intensities have been considered for the calculations are very small and do not present any preferential orientation in the two samples (i.e., N_{hkl} values smaller than 0.16 in all cases). Considering these data, we will refer to the (001) planes for the use of FT-IR data to account for preferential orientation phenomena.

B. FT-IR analysis of TiO_2 thin films

Figure 3 shows the IR absorption spectra of TiO_2-300 and TiO_2-600 samples taken at different incident angles. The series of bands appearing in these spectra are attributed to lattice vibrational modes. Their assignment according to the data reported in the literature for anatase[24] appear in Table IV. The sample TiO_2-300 are characterized by two bands at 262 and 435 cm^{-1} ascribed to the transverse optical phonons. There is also a feature, corresponding to the longitudinal modes in the spectral region from 750 to 830 cm^{-1}, which becomes more prominent at higher incidence angles. The spectrum of sample TiO_2-600 displays similar bands at normal incidence. However, the largest difference of these spectra compared with the previous ones is the shape of the band corresponding to longitudinal mode measured at highest incidence angles. In the high temperature samples, a well defined maximum appear at 856 cm^{-1} for incidence angles larger than 45°.

A proper analysis of the IR spectra at different incidence angles with incident polarized light can give information about the preferential orientation of crystal planes. Figure 4 shows the FT-IR absorption spectra of TiO_2-300 and TiO_2-600 samples recorded with *s*-(perpendicular) and *p*-(parallel) polarized light. In this case only the spectral region from 400 to 1000 was accessible to the analysis due to the absorbance of the KBr polarizer at lower frequencies. The spectra of the TiO_2-300 sample have the same aspect as those in Fig. 3 (taken with unpolarized light), either for parallel and perpendicular polarization. However, in the case of the sample TiO_2-600, although the spectra for *s* polarization do not depict any significant difference with the incidence

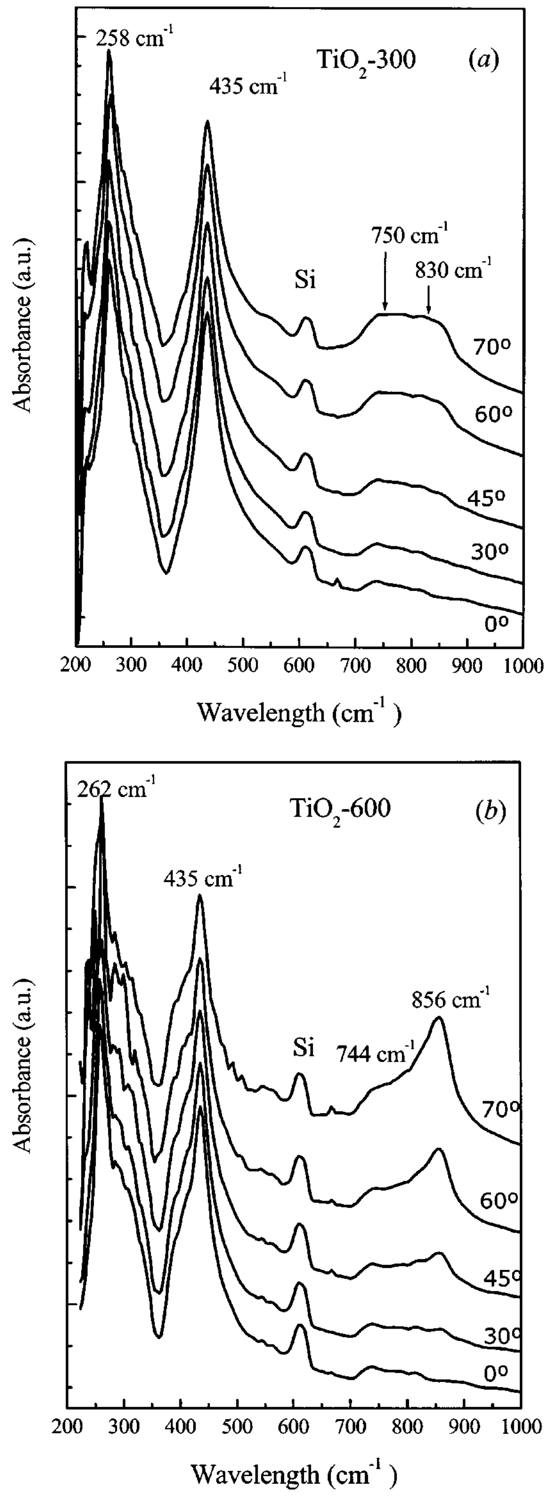

FIG. 3. Experimental absorbance of anatase thin layers prepared at 300 °C (a) and 600 °C (b) measured with unpolarized light. The band corresponding to the Si substrate has been marked.

TABLE IV. Vibrational IR modes of anatase.

Symmetry	Transverse frequency ω_T (cm^{-1})	Longitudinal frequency ω_L (cm^{-1})
E_u	262	366
E_u	435	876
A_{2u}	367	755

angle of the radiation, those for *p* polarization show a net enhancement of the longitudinal mode at 856 cm^{-1}, in a way similar to that found in the spectra with unpolarized light.

V. DISCUSSION

To interpret the absorbance of thin layers of anatase we have calculated the theoretical absorbance of anatase thin films deposited on silicon by the above described model by using its IR optical constants, measured by González *et al.*[24] The calculated theoretical absorbance spectra corresponding to two different crystallite orientations and several different incidence angles for *p*-polarized light are displayed in Fig. 5. The spectra calculated for *s*-polarized light were omitted because they do not appreciably change with incidence angle.[1] In the first case considered $c_{pez}=1/9$, the thin layer is anisotropic and composed of crystallites whose optical *c* axes is preferentially tilted 90° to the normal surface vector. In this case, two large maxima of absorbance with small shoulders are present at 242 and 440 cm^{-1} corresponding to the transverse optical (TO) E_u phonons[24] (258 and 435 cm^{-1}). At high values of incidence angle, an absorbance band ranging from 750 to 900 cm^{-1} is clearly visible. The maximum of this band shifts from 835 to 875 cm^{-1} for higher values of incidence angle. This final value corresponds to the highest frequency longitudinal E_u phonon (876 cm^{-1}).

In the case where the crystallites are randomly oriented, $c_{pez}=1/3$, it can be seen that the general aspect of the absorbance curves in the region of transverse modes are similar to those of $c_{pez}=1/9$. However, in the spectral area of longitudinal frequencies corresponding to high incidence angle spectra, the maximum of the longitudinal E_u phonon (876 cm^{-1}) is now flanked by the longitudinal A_{2u} mode (755 cm^{-1}), which now appears as a shoulder at 800 cm^{-1}.

In Fig. 5 we have also plotted the absorbance curves corresponding to $c_{pez}=7/9$, which represents the case of crystallites with its *c* axes preferentially orientated parallel to the normal of the surface sample. In this situation, the spectral region from 200 to 600 cm^{-1} displays two strong absorbance bands corresponding to the E_u-TO modes. However, the high frequency band corresponding to the longitudinal optical (LO) phonons is different. In this case, the A_{2u} mode (755 cm^{-1}) is similar or even more prominent than the E_u (876 cm^{-1}) especially in case of the largest incidence angles.

The use of Table I in addition to a close observation of the spectral region corresponding to the LO modes could help to determine if an anisotropic polycrystalline sample is textured. In the case that $c_{pez}<1/3$ we see in Table I that along the *z* axis the dielectric tensor takes the value of the ordinary dielectric constant. It implies that at higher incidence angles and with parallel polarization, only the LO frequencies of modes of degeneracy 2 could be visible (i.e., E_u modes). If $c_{pez}=1/3$, the sample is isotropic and under both parallel and perpendicular polarization the same spectra should be obtained at grazing angles. Finally, when $c_{pez}>1/3$ the spectral area corresponding to the LO modes measured at high incidence angles and under parallel polarization are dominated by the longitudinal extraordinary modes. This simple scheme agrees very well with the experimental data. For the sample prepared at 300 °C and measured at high incidence angles with the polarized light (Fig. 4), bands around 800 cm^{-1} appear similar to those of theoretical spectra calculated for $c_{pez}=1/3$. In this sample no indication of anisotropy was found since the spectra recorded with both the parallel and perpendicular components of the polarized spectra were similar [Figs. 4(a) and 4(c)]. On the contrary, the sample prepared at 600 °C, parallel and perpendicular polarized spectra are no longer similar. In this case, the composite exhibits a true anisotropic behavior. The shape of the LO band indicates that the E_u (876 cm^{-1}) mode is active at higher incidence angles in agreement with a partial orientation of the sample corresponding to $c_{pez}<1/3$.

Spectra taken with unpolarized light (Fig. 3), are experimentally easier to record, but cannot be used to perform quantitative analysis because they are a linear combination of parallel and perpendicular components. However, from a qualitative point of view, it should be noted that unpolarized spectra at higher angles (60° and 70°) (Fig. 3) look similar to those taken with the parallel component of the electric field but at a lower angle (50°) [Figs. 4(a) and 4(b)]. Thus, it can be concluded that unpolarized spectra taken at near grazing angles have qualitative but valuable information about textures in the region of longitudinal modes in a way similar to the parallel polarized spectra.

According to our interpretation of IR spectra, it seems that *c* axes of crystallites of the TiO_2-600 sample present a certain preferential orientation parallel to its external surface, a fact that is corroborated by x-ray diffraction results. This orientation corresponds to a preferential growth of (101) planes parallel to the surface. The crystallographic *c* axis of the anatase structure ($a=3.776$ and $c=9.486$ Å) forms an angle of $\phi_{(101)}=21.70°$ with respect to the (101) plane. Therefore, in the oriented (101) TiO_2-600 sample, the *c* axes of the crystallites describe a cone-shaped distribution around the azimutal axes perpendicular to the sample, being α_{th} the angle between the axis and the generatrix of the cone. According to Eq. (18), and taking $\alpha_{th}=90°-\phi_{(101)}=68.28°$, we get $c_{pez}=0.07$. This value is close to $c_{pez}=1/9=0.11$, whose IR theoretical spectra are represented in Fig. 4(a).

In order to get a closer view of the validity of the method, we have plotted together (Fig. 6) the experimental and calculated absorbance spectra (*p* polarization) of anatasa films for different incidence angles. The experimental plotted spectra correspond to samples heated at 300 and 600 °C and the theoretical ones to those calculated assuming that crystallites are oriented according to values of c_{pez}, 1/9 and 1/3 (random distribution). A direct comparison of the spectra reveals the advantages and weaknesses of the proposed method are clearly visible. Firstly, it should be noted that calculated spectra follow the same general trend as the experimental

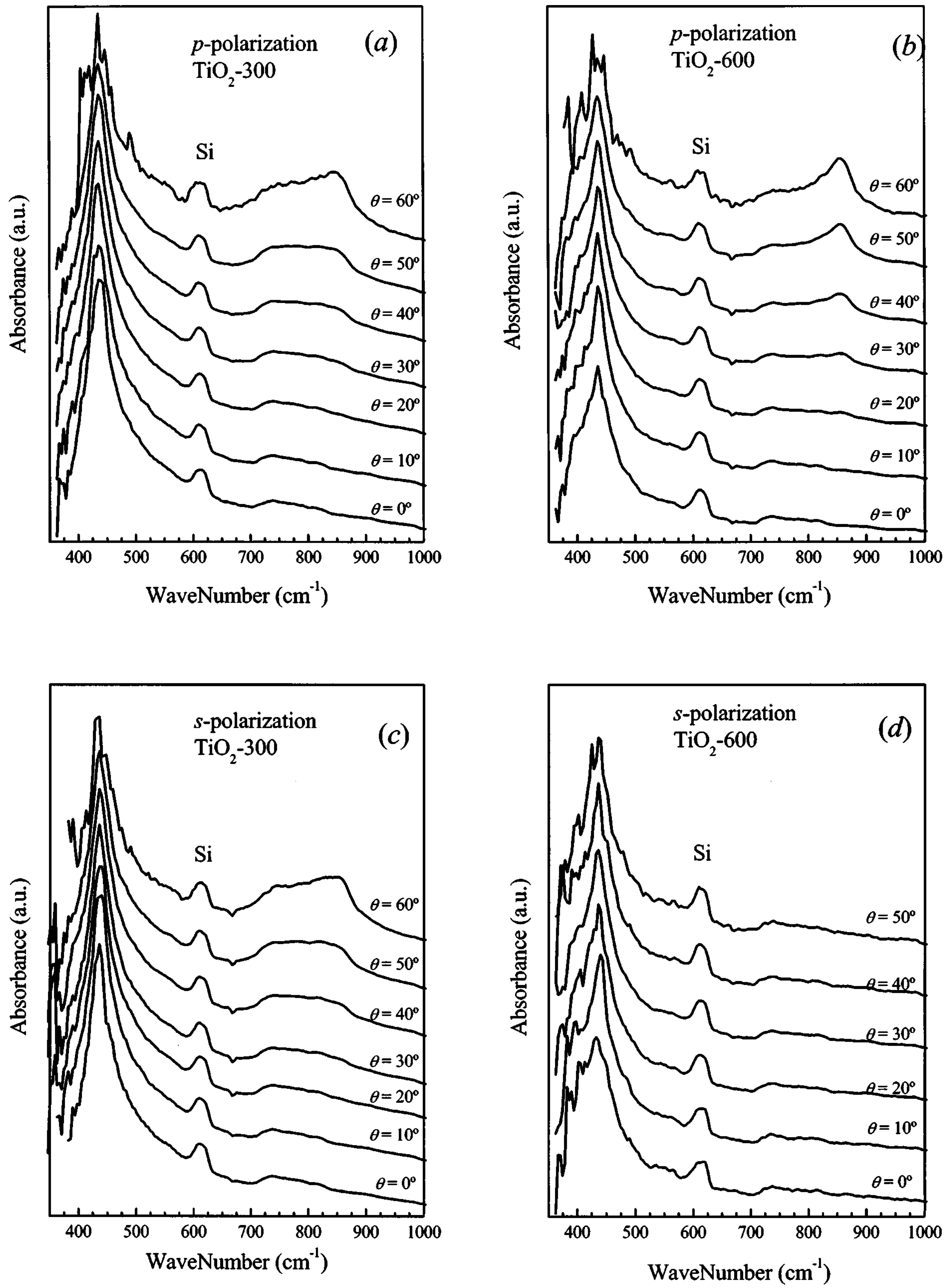

FIG. 4. Experimental absorbance of anatase thin layers prepared at 300 °C (a) and (c) and 600 °C (b) and (d) measured with parallel (a) and (b) and perpendicular light (c) and (d). The band corresponding to the Si substrate has been marked.

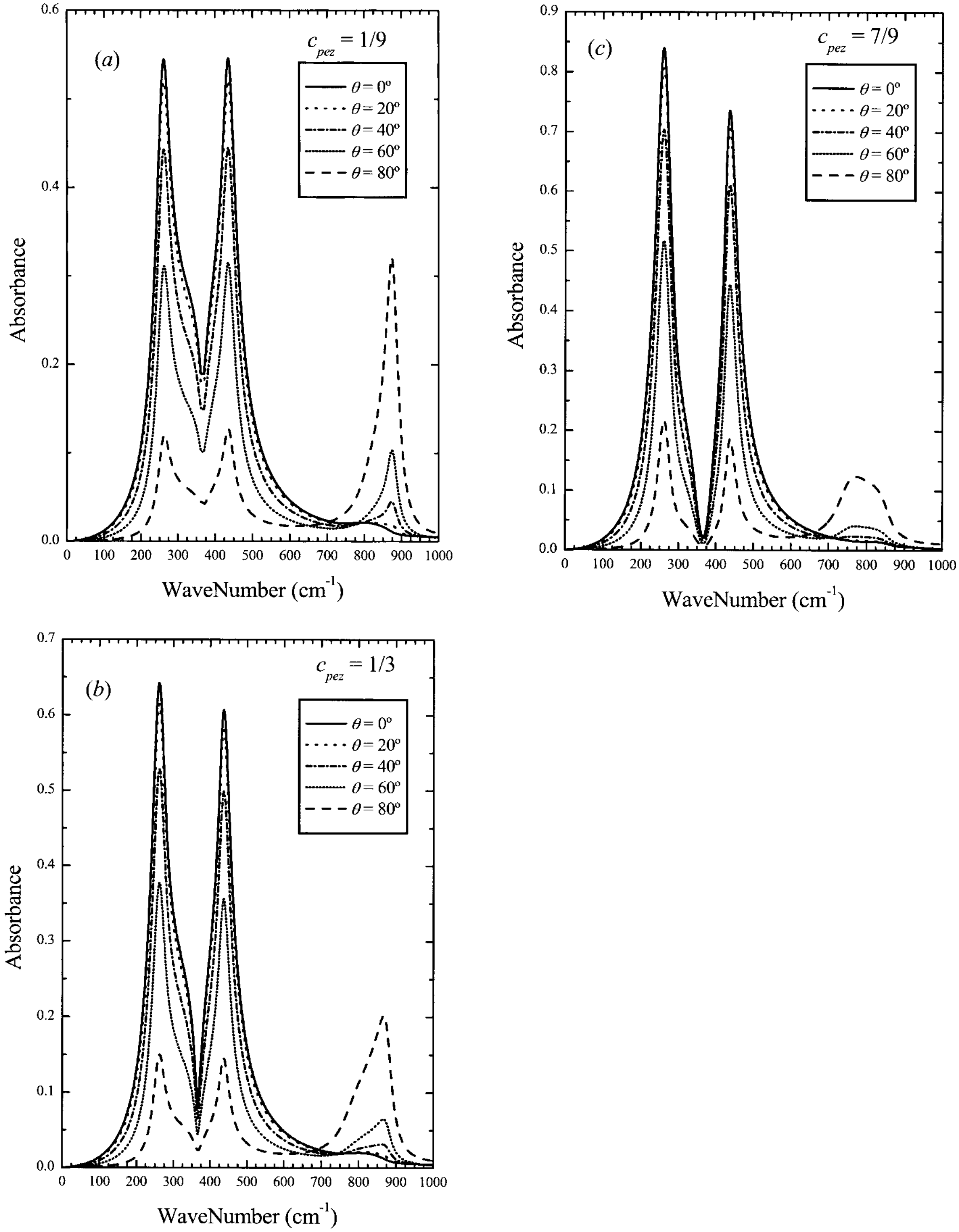

FIG. 5. Calculated values of absorbance for $L_p = 1/3$ and $c_{\mathrm{pez}} = 1/9$ (a), $c_{\mathrm{pez}} = 1/3$ (b), and $c_{\mathrm{pez}} = 7/9$ (c).

ones. However, discrepancies between them appear around 610 and 750 cm^{-1}. These bands are due to multiphonon processes of the silicon substrate.[25] In the same way, the longitudinal frequency of calculated spectra is shifted 25 cm^{-1} to higher frequencies in both kinds of samples. The origin of this mismatch remains unclear and we attribute it to absorbance fluctuations versus frequency of the silicon substrate in this spectral area,[25] or more likely, to a possible error in the fitted longitudinal frequency measured on the anatase single crystal.[24] In this sense, it should be noted that the calculated maximum of the high incidence angle curve exactly coincides with the longitudinal frequency of the anatase single crystal. Thus, in order to increase the accuracy of this method, in the future it will be necessary to properly characterize the substrate and to know with good precision the IR refractive index of the deposited film.

VI. CONCLUSIONS

In this article we have shown that longitudinal phonon modes measured by absorption infrared spectroscopy at grac-

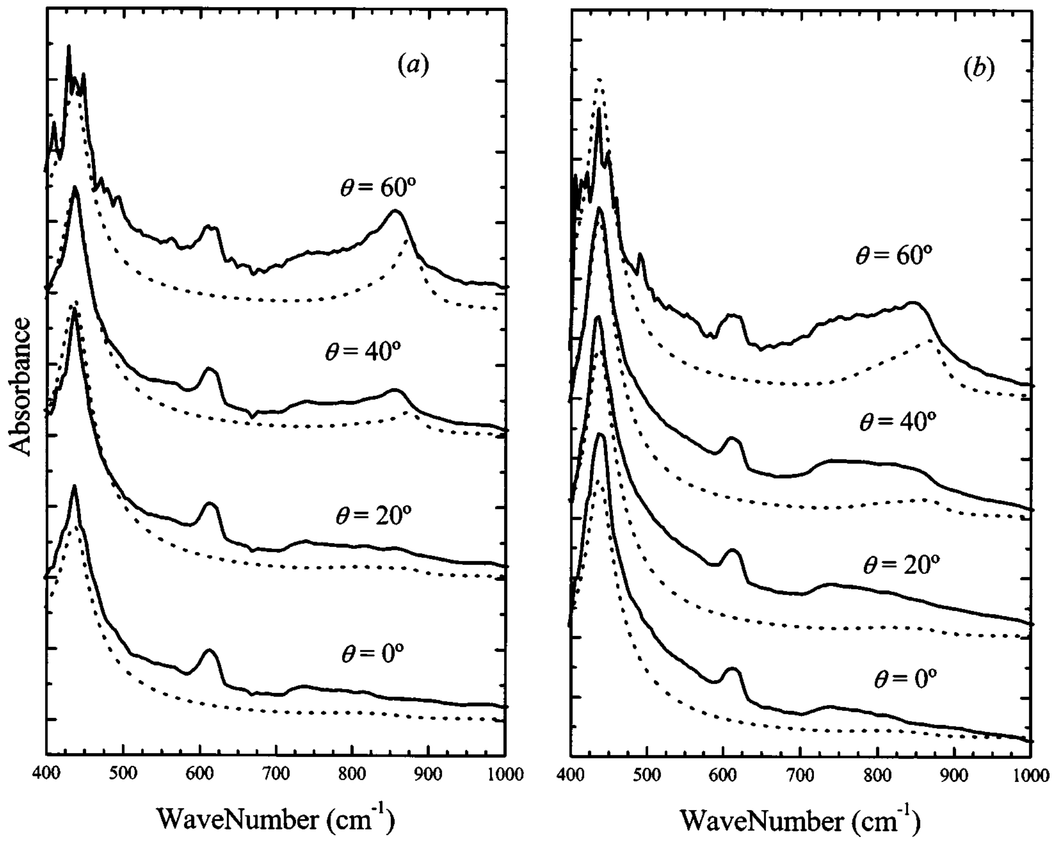

FIG. 6. Experimental (continuous line) absorbance curves of anatase thin films prepared at 600 °C (a) and 300 °C (b) and calculated (--) for $L_p = 1/3$ and $c_{pez} = 1/9$ (a), $c_{pez} = 1/3$ (b), at different incidence angles for *p*-polarized light.

ing angles can be used to determine the presence of textures in thin layers of uniaxial materials. A simple theoretical model has been introduced and it has been shown that it reproduces quite well all the features of these spectra. Texture information obtained from IR spectroscopy was similar to that afforded by conventional XRD treatment, which support the validity of our IR model. Therefore, IR spectroscopy could be used as a valuable quick test to detect the presence of textures in dense anisotropic samples.

APPENDIX A: VALIDITY OF THE EFFECTIVE MEDIUM APPROXIMATION FOR ANISOTROPIC COMPOSITES

The aim of this section is to describe the model employed to determine the effective dielectric tensor in heterogeneous materials composed of an isotropic phase (labeled as "*m*") and uniaxial crystallites (labeled as "*p*"). According to previous works,[12,9] the average dielectric function along the direction of the external electric field $\mathbf{E}_0$ of an heterogeneous system can be expressed as

$$\langle \in_0 \epsilon \rangle_{\mathbf{E}_0} = \frac{\int\int\int_V \mathbf{D}_{\mathbf{E}_0}(\mathbf{r}) d^3\mathbf{r}}{\int\int\int_V \mathbf{E}_{\mathbf{E}_0}(\mathbf{r}) d^3\mathbf{r}}, \tag{A1}$$

$$\in_0 \langle \epsilon \rangle_{\mathbf{E}_0} = \frac{(1-f)\langle \mathbf{D}_m \rangle_{\mathbf{E}_0} + f\langle \mathbf{D}_p \rangle_{\mathbf{E}_0}}{(1-f)\langle \mathbf{E}_m \rangle_{\mathbf{E}_0} + f\langle \mathbf{E}_p \rangle_{\mathbf{E}_0}}, \tag{A2}$$

where, $\langle D \rangle_{\mathbf{E}_0}$ and $\langle E \rangle_{\mathbf{E}_0}$ are, respectively, the space average of the displacement and electric field in the direction of the external applied field $\mathbf{E}_0$ and $\in_0$ is the vacuum permittivity. These expressions are valid when the particle size is much smaller than the incident wavelength radiation. In order to estimate these averages it has been assumed that individual particles are ellipsoids, whose geometric axes are parallel to the optical ones and that the external field around these particles is homogeneous (effective medium hypothesis).

To determine the effective dielectric constant as it appears in Eq. (A1) it is necessary to relate the internal particle field $\mathbf{E}_p$ with the external average value $\langle E \rangle_{\mathbf{E}_0}$. The link between both fields, determined by the Poisson equation corresponding to a spheroid of dielectric tensor $\boldsymbol{\epsilon}_p$ embedded in an anisotropic matrix, is characterized by its dielectric tensor $\langle \boldsymbol{\epsilon} \rangle$ under the effect of an external and homogeneous electric field. We will assume that the heterogeneous medium presents uniaxial behavior. This simplification allows us to describe the dielectric tensor by only two components: $\langle \epsilon_\parallel \rangle$ and $\langle \epsilon_\perp \rangle$, i.e., the effective dielectric constant in the direction parallel and perpendicular of the average field respectively. According to this reference frame, the dielectric tensor is given by

$$\tilde{\boldsymbol{\epsilon}}(\theta) = \begin{pmatrix} \langle \epsilon_\parallel \rangle - \Delta\epsilon \sin^2\theta & \langle \Delta\epsilon \rangle \sin\theta\cos\theta \\ \langle \Delta\epsilon \rangle \sin\theta\cos\theta & \langle \epsilon_\parallel \rangle - \langle \Delta\epsilon \rangle \cos^2\theta \end{pmatrix}, \tag{A3}$$

where θ is the angle of the ray direction in respect to the optical axis of the crystallite, and $\langle\Delta\epsilon\rangle$ is given by

$$\langle\Delta\epsilon\rangle=\langle\epsilon_{\parallel}\rangle-\langle\epsilon_{\perp}\rangle. \tag{A4}$$

In order to simplify the expressions, we will assume that the anisotropic particles have a spherical shape. The solution of the Poison equation, applied to a spherical inclusion inside an anisotropic matrix can be approximated by

$$V(r,\theta)=\begin{cases} E_i r\cos\theta+\Delta V_i(r,\theta) & r<a \\ \langle E\rangle r\cos\theta+\mu\dfrac{\cos\theta}{r^2} & r>a \end{cases}. \tag{A5}$$

This potential is similar to that of the isotropic case except for the term ΔV_i, which takes into account the effect of the anisotropy of the space outside the sphere in it. This potential will induce an electric field ΔE_i. By applying boundary conditions into the sphere surface $(r=a)$ for the electric and displacement field we get

$$\begin{aligned} E_i|_{t,r=a}&=E_e|_{t,r=a}, \\ D_i|_{n,r=a}&=D_e|_{n,r=a}, \end{aligned} \tag{A6}$$

$$\frac{\Delta E_i}{E_i}=\frac{\langle\Delta\epsilon\rangle}{\langle\epsilon_{\parallel}\rangle}\sin^2\theta\left(\frac{\mu}{a^3}-2\langle E\rangle\right). \tag{A7}$$

Thus, the contribution of ΔE_i to the average electric field parallel to $\mathbf{E}_i$ is cancelled due to the symmetry of the field distribution

$$\langle\Delta E_i\rangle=\int_{V_p}\frac{\langle\Delta\epsilon\rangle}{\langle\epsilon_{\parallel}\rangle}E_i\left(\frac{\mu}{a^3}-2\langle E\rangle\right)\sin^2\theta\cos\theta\,dV=0. \tag{A8}$$

This latter expression indicates that, at least at the first order, the component of the electric field inside a spherical inclusion in the direction of the external applied field is not modified by the anisotropy of the external medium. This result allows us to extend the results of the effective medium approximation from isotropic to anisotropic media. Thus, the expressions previously obtained for isotropic heterogeneous media also apply for each l direction of an anisotropic composite [Eq. (1)].

Under these approximations the internal electric field for a single particle of the k phase (p or m) along the o direction is constant and given by

$$E_{ko}=\frac{\langle\epsilon\rangle_o}{(1-L_{ko})\langle\epsilon\rangle_o+L_{ko}\epsilon_{ko}}\langle E\rangle_o, \tag{A9}$$

where L_{kl} is the lth depolarization factor of a k ellipsoid. The space averaged field, parallel to the applied field along the o direction turns out to be

$$\begin{aligned}\langle E_{ol}\rangle_{\mathbf{E}_0}&=\frac{1}{V}\int_V E_{ol}(\mathbf{r})\,\gamma_{kl,\mathbf{E}_0}(\theta)d\mathbf{r} \\ &=\sum_{k=1}^{N} f_k E_{okl}\int_\Omega \gamma_{kl,\mathbf{E}_0}(\theta)d\Omega=4\pi\sum_{k=1}^{N} f_k E_{okl}c_{kl},\end{aligned} \tag{A10}$$

where f_k is the filling factor of the k phase, and $\gamma_{kl,\mathbf{E}_0}(\theta)$ is the density function corresponding to the probability of finding that the l axis of the ellipsoid makes an angle θ with $\mathbf{E}_0$. In this sense c_{kl} is the orientation average of the projection of the internal field to the direction of the external applied field

$$c_{kl}|_{\mathbf{E}_0}=\frac{1}{4\pi}\int_0^{2\pi}d\varphi\int_0^{\pi}\gamma_{kl,\mathbf{E}_0}(\theta)\sin\theta\,d\theta. \tag{A11}$$

The same calculation applies for the average displacement

$$\begin{aligned}\langle D_{ol}\rangle_{\mathbf{E}_0}&=\frac{1}{V}\int_V D_{ol}(\mathbf{r})\,\gamma_{kl,\mathbf{E}_0}(\theta)d\mathbf{r} \\ &=\sum_{k=1}^{N} f_k\epsilon_{okl}E_{okl}\int_\Omega\gamma_{kl,\mathbf{E}_0}(\theta)d\Omega \\ &=4\pi\sum_{k=1}^{N} f_k\epsilon_{okl}E_{okl}c_{kl}.\end{aligned} \tag{A12}$$

Finally, we get

$$\langle\epsilon\rangle_l=\frac{\Sigma_{k=1}^N f_k\Sigma_{o=1}^3\dfrac{c_{kol}\epsilon_{ko}}{(1-L_{ko})\langle\epsilon\rangle_l+L_{ko}\epsilon_{ko}}}{\Sigma_{k=1}^N f_k\Sigma_{o=1}^3\dfrac{c_{kol}}{(1-L_{ko})\langle\epsilon\rangle_l+L_{ko}\epsilon_{ko}}}. \tag{A13}$$

APPENDIX B

In this Appendix we want to show the explicit expressions derived from the "4×4 matrix transfer procedure" used in this work as described by Schubert *et al.*[21–23] These expressions have been employed to derive the theoretical absorbance curves plotted in Figs. 5(a)–5(c). The relationship between the incidence, reflected and transmitted beam depend on the geometric configuration of the samples[21] according to

$$\begin{pmatrix} A_s \\ B_s \\ A_p \\ B_p \end{pmatrix}=\mathbf{T}\begin{pmatrix} C_s \\ 0 \\ C_p \\ 0 \end{pmatrix}, \tag{B1}$$

where A_s, A_p, B_s, B_p, C_s, and C_p are the complex amplitudes of the parallel and perpendicular modes of the incident, reflected, and transmitted waves, respectively. $\mathbf{T}$ is the transfer matrix, which can be written as the product of the incident, exit and layer matrix

$$\mathbf{T}=\mathbf{L}_a^{-1}\prod_{k=1}^{N}\mathbf{T}_{pk}^{-1}\mathbf{L}_f. \tag{B2}$$

In our case we only have a single layer $(N=1)$. The values of the matrices for a thin film of an uniaxial layer of thickness d, are given by[21]

$$\mathbf{T}_p^{-1}=\begin{pmatrix} \cos(k_0N_{xz}d) & 0 & 0 & -i\dfrac{N_{xz}}{\epsilon_x}\sin(k_0N_{xz}d) \\ 0 & \cos(k_0N_{yy}d) & -\dfrac{i}{N_{yy}}\sin(k_0N_{yy}d) & 0 \\ 0 & iN_{yy}\sin(k_0N_{yy}d) & \cos(k_0N_{yy}d) & 0 \\ -i\dfrac{\epsilon_x}{N_{xz}}\sin(k_0N_{xz}d) & 0 & 0 & \cos(k_0N_{xz}d) \end{pmatrix}, \tag{B3}$$

$$\mathbf{L}_a^{-1}=\frac{1}{2}\begin{pmatrix} 0 & 1 & \dfrac{-1}{n_i\cos\theta_i} & 0 \\ 0 & 1 & \dfrac{1}{n_i\cos\theta_i} & 0 \\ \dfrac{1}{\cos\theta_i} & 0 & 0 & \dfrac{1}{n_i} \\ \dfrac{-1}{\cos\theta_i} & 0 & 0 & \dfrac{1}{n_i} \end{pmatrix}, \tag{B4}$$

$$\mathbf{L}_f=\begin{pmatrix} 0 & 0 & \cos\theta_s & 0 \\ 1 & 0 & 0 & 0 \\ -n_s\cos\theta_s & 0 & 0 & 0 \\ 0 & 0 & n_s & 0 \end{pmatrix}, \tag{B5}$$

where $k_0=2\pi/\lambda$ is the wave vector, ϵ_x and ϵ_z are the relative dielectric constant of the layer perpendicular and parallel to the normal to the plane, n_i and n_s are the refractive index of the incident medium and substrate, and θ_i and θ_s are the incidence and transmitted angles. Finally, the terms N_{xx}, N_{yy}, and N_{xz} are defined following Ref. 21

$$N_{xx}=N_{yy}=\sqrt{\epsilon_x-\epsilon_i\sin^2\theta_i},$$
$$N_{yy}=\sqrt{\epsilon_x-\frac{\epsilon_i\epsilon_x}{\epsilon_z}\sin^2\theta_i}. \tag{B6}$$

The final product $\mathbf{T}$ has all coefficients equal to zero except for T_{11}, T_{21}, T_{33}, and T_{43}.

$$\mathbf{T}=\mathbf{L}_a^{-1}\mathbf{T}_{pk}^{-1}\mathbf{L}_f=\begin{pmatrix} T_{11} & 0 & 0 & 0 \\ T_{21} & 0 & 0 & 0 \\ 0 & 0 & T_{31} & 0 \\ 0 & 0 & T_{43} & 0 \end{pmatrix}. \tag{B7}$$

Thus, the transmission and reflection coefficients, parallel and perpendicular are given by[19]

$$\begin{pmatrix} A_s \\ B_s \\ A_p \\ B_p \end{pmatrix}=\begin{pmatrix} T_{11} & 0 & 0 & 0 \\ T_{21} & 0 & 0 & 0 \\ 0 & 0 & T_{31} & 0 \\ 0 & 0 & T_{43} & 0 \end{pmatrix}\begin{pmatrix} C_s \\ 0 \\ C_p \\ 0 \end{pmatrix}, \tag{B8}$$

$$t_s=\left(\frac{C_s}{A_s}\right)_{A_p=0}=\frac{1}{T_{11}} \quad r_s=\left(\frac{C_s}{B_s}\right)_{A_p=0}=\frac{1}{T_{21}}, \tag{B9}$$

$$t_p=\left(\frac{C_p}{A_p}\right)_{A_s=0}=\frac{1}{T_{33}} \quad t_p=\left(\frac{C_p}{B_p}\right)_{A_s=0}=\frac{1}{T_{43}}.$$

Finally the optical absorbance is given by

$$\mathcal{A}_{s,p}=-\log_{10}(|t_{s,p}|^2). \tag{B10}$$

[1] D. W. Berreman, Phys. Rev. **130**, 2193 (1963).
[2] H. D. Riccius, J. Appl. Phys. **19**, 4381 (1968).
[3] F. Proix and M. Balkanski, Phys. Status Solidi **32**, 119 (1969).
[4] H. Poulet and J. P. Mathieu, *Vibration Spectra and Symmetry of Crystals* (Gordon and Breach, New York, 1976), p. 238.
[5] S. Hayashi, N. Nakamori, and H. Kanamori, J. Phys. Soc. Jpn. **46**, 176 (1979).
[6] I. L. Skryabin, A. V. Radchik, P. Moses, and G. B. Smith, Appl. Phys. Lett. **70**, 2221 (1997).
[7] M. Schubert, B. Rheinländer, E. Franke, H. Neumann, T. E. Tiwald, J. A. Woollam, J. Hahn, and F. Richter, Phys. Rev. B **56**, 13306 (1997).
[8] E. Franke, M. Schubert, H. Neumann, T. E. Tiwald, D. W. Thompson, J. A. Woollam, J. Hahn, and F. Richter, J. Appl. Phys. **82**, 2906 (1997).
[9] C. Pecharromán and J. E. Iglesias, Appl. Spectrosc. **54**, 634 (2000).
[10] F. Yubero, M. Ocaña, A. Justo, L. Contreras, and A. R. Gonzalez-Elipe, J. Vac. Sci. Technol. A **18**, 2244 (2000).
[11] J. P. Espinós, A. Fernández, A. Caballero, V. M. Jiménez, J. C. Sánchez-López, L. Contreras, D. Leinen, and A. R. González-Elipe, Adv. Mater. **3**, 219 (1997).
[12] C. Pecharromán and J. E. Iglesias, Phys. Rev. B **49**, 7137 (1994).
[13] P. E. Sulewski, T. W. Noh, J. T. McWhirter, and J. Sievers, Phys. Rev. B **36**, 5735 (1987).
[14] T. W. Noh, P. H. Song, and A. J. Sievers, Phys. Rev. B **44**, 5459 (1991) and references in therein.
[15] D. A. G. Bruggerman, Ann. Phys. (Leipzig) **24**, 636 (1935).
[16] R. Landauer, J. Appl. Phys. **23**, 770 (1952).
[17] M. Born and E. Wolf, *Principles of Optics*, 6th ed. (Pergamon, Oxford, 1983).
[18] D. W. Berreman, J. Opt. Soc. Am. **62**, 502 (1972).
[19] P. Yeh, Surf. Sci. **96**, 41 (1980).
[20] M. Schubert, Thin Solid Films **313**, 323 (1998).
[21] M. Schubert, T. E. Tiwald, and C. M. Herzinger, Phys. Rev. B **61**, 8187 (2000).
[22] A. Kreuter, G. Wagner, K. Otte, G. Lippold, A. Schindler, and M. Schubert, Appl. Phys. Lett. **78**, 195 (2001).
[23] M. Schubert, Phys. Rev. B **53**, 4265 (1996).
[24] R. J. González, R. Zallen, and H. Berger, Phys. Rev. B **55**, 7014 (1997).
[25] D. F. Edwards, in *Handbook of Optical Constants of Solids*, edited by E. D. Palik (Academic, Orlando, FL, 1985), pp. 547–569.